N89-27748

88-064

RING CUSP/HOLLOW CATHODE DISCHARGE CHAMBER PERFORMANCE STUDIES*

J. A. Vaughn+ and P. J. Wilbur†
Colorado State University
Fort Collins, Colorado U.S.A.

ABSTRACT

An experimental study performed to determine the effects of hollow cathode position, anode position and ring cusp magnetic field configuration and strength on discharge chamber performance, is described. The results are presented in terms of comparative plasma ion energy cost, extracted ion fraction and beam profile data. Such comparisons are used to demonstrate whether changes in performance are caused by changes in the loss rate of primary electrons to the anode or the loss rate of ions to discharge chamber walls or cathode and anode surfaces. Results show 1) the rate of primary electron loss to the anode decreases as the anode is moved downstream of the ring cusp toward the screen grid, 2) the loss rate of ions to hollow cathode surfaces are excessive if the cathode is located upstream of a point of peak magnetic flux density at the discharge chamber centerline, and 3) the fraction of the ions produced that are lost to discharge chamber walls and ring magnet surfaces is reduced by positioning of the magnet rings so the plasma density is uniform over the grid surface and adjusting their strength to a level where it is sufficient to prevent excessive ion losses by Bohm diffusion.

INTRODUCTION

A study conducted by Hiatt[1] on a specially designed 8 cm dia. ring cusp magnetic field ion source has shown the effects of the positions of a loop filament cathode and loop anode on discharge chamber performance. Based on this work it was concluded that the performance of a ring cusp discharge chamber is best when 1) the surface of revolution of the innermost magnetic field line that intercepts the anode (i.e. the virtual anode surface) also intercepts the outermost ring of holes in the screen grid and 2) the surface of revolution of the outermost field line that intercepts the outer boundary of the electron source (i.e. the virtual cathode surface) is located relative to the virtual anode so that the discharge is on the threshold of extinction at the prevailing discharge voltage. Hiatt used a refractory filament cathode in his study because it was convenient and it could be positioned to control precisely the virtual cathode surface (i.e. the field line surface of revolution on which primary electrons are released into the discharge chamber). The study presented in this paper is similar in focus to the one conducted by Hiatt, but hollow cathodes, which are better suited for long life space applications, are used in place of the refractory filament cathodes used by Hiatt. The objective of this study has been to develop an understanding of the mechanisms whereby the field strength and location of ring cusp fields and the location of the hollow cathode and anode relative to these fields influence discharge chamber performance.

The tests were conducted on a small (7 cm diameter) ion source that utilizes high flux density magnets. The use of these magnets in such a small source produced fields that penetrated deep into the chamber and as a result the volume of the low magnetic flux density zone in the chamber was small. It is difficult to achieve good performance in such a chamber, but the sensitivity of its performance to changes in such parameters as cathode and anode position is great and it was believed this would make it easier to identify the effects of changes and gain an understanding of the phenomena and mechanisms involved.

APPARATUS AND PROCEDURE

A cross sectional view of the 7.0 cm dia. multiple ring cusp discharge chamber used in the study is shown in Fig. 1. It was designed as a flexible research tool in which the dimensions labeled could be varied to determine their effect on performance. For this study, however, the steel discharge chamber diameter and length ℓ_d and the beam diameter d_b were all held constant at 9.0 cm, 5.0 cm and 7.0 cm respectively. This short 5.0 cm discharge chamber was used to provide the flexibility necessary to position the hollow cathode both upstream and downstream of the ring cusp magnet reference location shown near the middle of the chamber. The magnetic field in the discharge chamber was produced by two radially facing ring magnets with their mid lines located 0.3 cm and -3.0 cm upstream of the screen grid and one axially facing ring magnet surrounding the hollow cathode and located on the upstream end of the discharge chamber. The central ring magnet, which is located a distance ℓ_r upstream of the grids, was varied during one test, but the ring magnet nearest the screen grid and the one on the

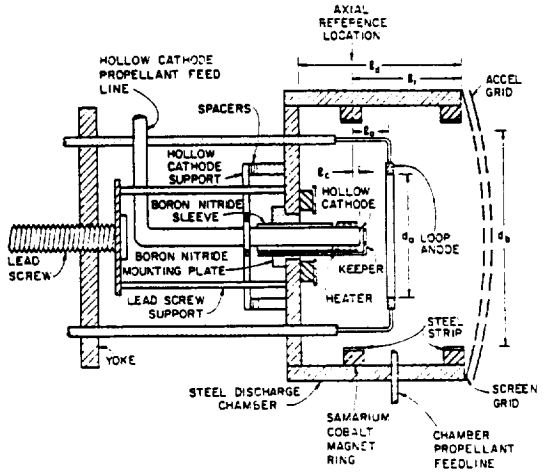

Fig. 1. Cross Sectional View of Ring Cusp Ion Source

*Work Supported by NASA Grant NGR-06-002-112
+Research Assistant, Department of Mechanical Engineering, Student Member AIAA
†Professor, Department of Mechanical Engineering, Member AIAA

upstream face remained fixed throughout all tests. Note that the positions of the anode ℓ_a and cathode ℓ_c are measured with respect to the axial reference location at the center of the central (radially facing) ring magnet. Each ring magnet is made up of small (1.2 cm by 0.6 cm by 0.5 cm) samarium cobalt magnet segments with a strength of 0.27 T at their surfaces. The rings were formed by placing the magnet segments end-to-end either around the inner circumference of the discharge chamber (radially facing magnets) or in a circular pattern with an approximate diameter of 3.0 cm (upstream magnet). The steel strips and the washer, which are shown covering the radial and axially facing magnets respectively in Fig. 1, were used to distribute the magnetic flux uniformly over each ring surface during a test in which the numbers of magnet segments in each ring were varied and the effects of magnetic flux density on discharge chamber performance were investigated. The tantalum loop anode shown in Fig. 1 has a fixed diameter d_a of 5.2 cm and under the action of the lead screw and yoke it can be moved either upstream or downstream of the axial reference location. Because anode locations upstream of this location resulted in very poor performance and instabilities that prevented data collection, results pertaining only to downstream anode locations (positive values of ℓ_a) will be presented.

A 0.64 cm dia tantalum tube was electron beam welded to a tungsten orifice plate with a 0.76 mm dia orifice to form the hollow cathode shown in Fig. 1. It utilized a R-500 treated rolled tantalum foil insert and was equipped with a swaged heater to facilitate startup. As the figure suggests the cathode is mounted in an electrically insulating boron nitride mounting plate/sleeve assembly, which keeps it isolated electrically but allows it to be moved axially from one test to the next by changing spacers at the cathode supports. This assembly is sufficiently leak tight to prevent significant propellant leakage from the discharge chamber into the vacuum system. The cathode orifice plate can be moved upstream (negative ℓ_c) and downstream (positive ℓ_c) of the axial reference location. The toroidal tantalum keeper shown in Fig. 1 has a 0.16 cm minor diameter and a 0.32 cm major diameter, is positioned 0.8 mm downstream of the hollow cathode orifice plate and is supported by the boron nitride mounting plate.

Xenon propellant which has been used in all tests was supplied through both the hollow cathode and the main propellant feed line. The total flow-rate into the chamber, used to compute propellant efficiencies and neutral atom loss rates, reflected both of these measured flows as well as the backflow of xenon from the vacuum chamber through the grids.[2]

The dished small hole accelerator grid (SHAG) optics set has screen and accel hole diameters of 1.9 mm and 1.5 mm, respectively, and these holes are arranged with a 2.2 mm centerline to centerline spacing. The cold grid spacing was 0.6 mm and the grids were maintained at 750 V (screen grid) and -250 V (accel grid) for all tests. The experiments were conducted in a 46 cm dia bell jar which was diffusion pumped to a background pressure in the low 10^{-6} Torr range. Typical operating pressures were in the high 10^{-5} to low 10^{-4} range over the range of xenon flows used in the tests.

A Faraday probe was swept through the beam 4 cm downstream of the accel grid to measure beam current density profiles. The probe consists of a 0.6 cm dia molybdenum ion current sensing disc that is shielded from the beam plasma electrons by a stainless steel screen biased 9 V below ground potential and is enclosed in a stainless steel body. Figure 2 shows a typical beam current density profile; this one was measured at a 100 mA beam current (J_B) and the other conditions defined in the legend by simultaneously inputing the ion current signal from the probe sensor and radial position of the probe to an x-y recorder. Current density profiles were analyzed numerically to determine the beam flatness parameter and total beam current (i.e., the integrated beam current) associated with the profile. Integrated beam currents were always found to agree with directly measured beam currents to within ± 10 %. The beam flatness parameter is a measure of the uniformity of the beam profile and is defined as the average-to-maximum beam current density ratio measured close to the grids.

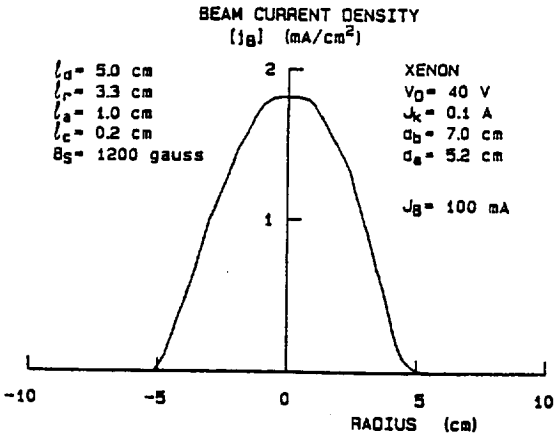

Fig. 2. Typical Beam Current Density Profile

The magnetic field configuration of a discharge chamber has been found to have a major influence on the performance of that chamber and it is frequently important that the field prevailing in a chamber during a test be described. This can be accomplished by using iron filings maps and flux density contour maps measured in the actual chamber. During the conduct of this work, however, it was determined that a computer algorithm developed by Arakawa[3] could be used to generate both types of maps reliably, quickly and with relative ease so it has been used to generate the maps contained in this paper. The computer algorithm allows the user to enter parameters which describe the discharge chamber geometry, the permanent magnet locations in the discharge chamber and their magnetization levels. The program then solves for the magnetic field vector potential at each element using the finite element method. The magnetic field vector potential can be plotted as a function of position in the discharge chamber to produce a computer-generated (pseudo) iron filings map like the one shown in Fig. 3. This particular map was produced for a flux density measured at the surface of the steel strips B_S of 1200 gauss and the geometric data shown in the legend. Because the computer program generates an axis-symmetric view, only half of the map is plotted. By taking the gradient of the vector potential map the program can also be used to generate a constant flux density contour map. Figure 4 is a typical example of such a computer-generated magnetic flux density contour map for the same discharge chamber and magnet configuration that produced the filings map shown in Fig. 3. It should be noted that the contours shown decrease logarithmically with distance from the discharge

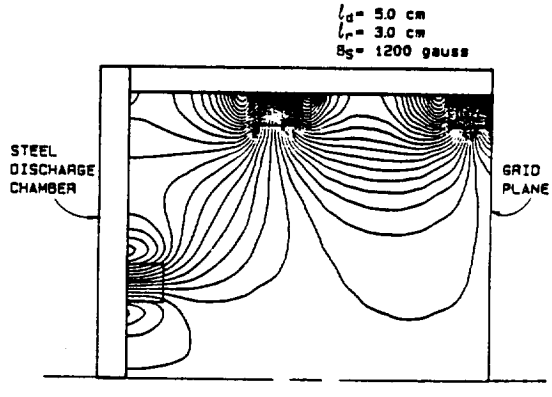

Fig. 3. Pseudo Iron Filings Map (Computer Generated)

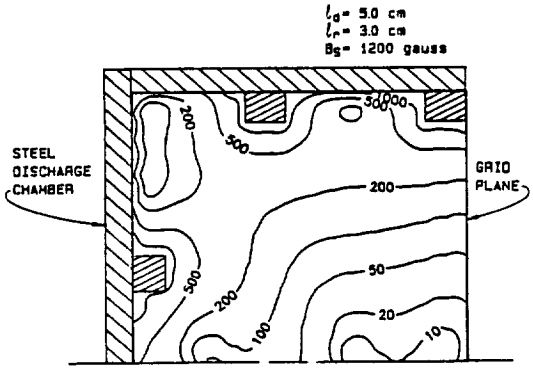

Fig. 4. Magnetic Flux Density Contour Map (Computer Generated)

chamber walls. Maps like those shown in Figs. 3 and 4 can be used to explain the effects of magnetic field changes on discharge chamber performance. They make it possible to view the effects of changing ring magnet positions and strengths on magnetic field line patterns and flux densities in the discharge chamber.

Tests were initiated by flooding the hot hollow cathode with xenon propellant and then applying a sufficiently high keeper voltage (~200 V) to start a keeper discharge. After startup the keeper voltage was varied as required to maintain a 0.1 A keeper current for all testing. The cathode flowrate was reduced once the keeper discharge had started and a discharge to the anode, which was held at a 40 V potential, was established. The current being drawn to the anode was maintained at approximately an ampere by controlling the main and/or cathode flowrates until thruster operation had stabilized. After a period of stabilization, tests were typically conducted by setting the xenon flowrate through the hollow cathode to ~ 20 mA eq (Xe) and that into the discharge chamber to ~ 95 mA eq (Xe) while maintaining the discharge voltage V_D at 40 V. The cathode and discharge chamber flowrates $\dot{m}_c$ and $\dot{m}_d$, the vacuum chamber background pressure P_o, the keeper voltage V_K, the discharge current J_D, beam current J_B, and total ion production rate expressed as a current J_P, corresponding to this operating condition were all measured and recorded. Measurement of the total ion production current was accomplished by biasing the discharge chamber walls and screen grid 30 V negative of the hollow cathode to repel all electrons from these surfaces and sensing the ion current arriving at the discharge chamber magnet and wall surfaces J_W and the screen grid J_S. These two surfaces were isolated from each other so the currents of ions to each surface could be separated. The sum of these two currents plus the beam current is the total ion production current.

$$J_P = J_W + J_S + J_B \qquad (1)$$

Knowing the total ion production current the plasma ion energy cost ϵ_P (the energy cost of producing an ion in the plasma) and the extracted ion fraction f_B (the fraction of the total ions produced in the discharge chamber that are being extracted into the beam) could be computed using the expressions

$$\epsilon_P = \frac{V_D(J_D - J_P)}{J_P} \qquad (2)$$

and,

$$f_B = \frac{J_B}{J_P} \qquad (3)$$

The loss rate of neutral atoms through the grids, which is proportional to the discharge chamber atomic density and is therefore called the neutral density parameter, was also computed using

$$\dot{m}(1 - \eta_u) = \dot{m}_c + \dot{m}_d + \frac{P_o A_b \phi_o e}{\sqrt{2\pi m_i k T_o}} - J_B. \qquad (4)$$

In this equation, A_b the area of the beam, ϕ_o the transparency of the grids to neutral atom back flow, m_i the atom/ion mass, k Boltzmann's constant, e the electronic charge and T_o the ambient (vacuum chamber) neutral atom temperature are all known.

After all the currents (J_D, J_B and J_P), the voltage (V_K) and other data had been recorded at the initial flow condition, the discharge chamber flowrate was increased while the hollow cathode flowrate and discharge voltage were held constant. This caused the discharge current and hence the other currents and keeper voltage to change and their new values were recorded. This process of increasing discharge chamber flowrate and recording data was continued until the accel grid impingement current increased to ~10 mA. The hollow cathode and discharge chamber flowrates were then both reduced and the process of recording data, as the discharge chamber flowrate was increased incrementally and the cathode flowrate and discharge voltage were held constant, was continued. This process of reducing the hollow cathode flowrate and increasing the discharge chamber flowrate incrementally continued until data had been recorded over a wide range of discharge chamber neutral atom density levels (and therefore a wide range of discharge currents) at the prescribed 40 V discharge voltage. Typically, the hollow cathode flowrate had to be decreased from 20 to 10 mA eq (Xe) while the discharge chamber flowrate had to be increased from 95 to 460 mA eq (Xe) to cover an adequate range of neutral atom densities.

The effects of varying the position of the anode and the hollow cathode were investigated by first placing the cathode at a particular location in the discharge chamber and then moving the anode downstream in increments (i.e. onto field lines located progressively further from the virtual cathode). At each anode position, plasma ion energy cost and extracted ion fraction data were recorded as a function of neutral density parameter using the procedure described in the preceeding paragraph. This process continued until the anode was so far downstream of the cathode that the discharge currents drawn to the anode were small. The cathode was then repositioned and the process of moving the anode and varying the flowrates was repeated. The range of cathode positions investigated was from 0.6 cm upstream (ℓ_c = -0.6 cm) to 0.5 cm downstream (ℓ_c = 0.5 cm) of the reference location.

A second set of experiments was conducted in which the effects of varying the magnetic flux density B_s at the surfaces of both the steel strips and the washer covering the ring magnets was investigated. The magnetic flux density was varied by removing individual samarium cobalt magnet segments from each ring magnet and placing a steel strip or washer of sufficient thickness to produce a common, uniform surface magnetic flux density over the entire surface of each ring magnet. This required that the thickness of the strips and the washer be increased as the surface magnetic flux density was decreased in increments from 2700 gauss to 350 gauss. At each magnetic flux density condition plasma ion energy cost and extracted ion fraction data were recorded as a function of discharge chamber neutral density parameter using the experimental procedure described previously.

A final experiment was conducted in which the upstream ring magnet position (ℓ_r) was varied from 2.7 to 3.6 cm in increments of 0.3 cm to determine the effects of such changes on discharge chamber performance. The positions of the anode and hollow cathode were held constant relative to the reference location on this magnet during the test, so magnet ring, anode and cathode were all moved in unison. The procedures used to measure plasma ion energy cost data as a function of discharge chamber neutral density parameter were as described previously.

EXPERIMENTAL RESULTS

Experimentally measured discharge chamber performance can be described in terms of plasma ion energy cost ϵ_p vs. discharge chamber neutral density parameter $\dot{m}(1 - \eta_u)$ plots like the example shown in Fig. 5. These particular data were recorded using the discharge chamber having the configuration described by the parameters listed in the legend when the flux density B_S at the surface of each magnet was 1200 gauss.

The theory developed by Brophy[4] suggests the experimental data of Fig. 5 should be fitted by the equation

$$\epsilon_p = \epsilon_p^* (1 - \exp[-C_0 \dot{m}(1 - \eta_u)])^{-1} \qquad (5)$$

when the parameters ϵ_p^* (the baseline plasma ion energy cost) and C_0 (the primary electron utilization factor) are selected properly. In the case of the data shown in Fig. 5 a non-linear least-squares curve fit of the data yields the values of those parameters given on the figure. The data and the curve show a good correlation between the data and the model that is typical of all of the results obtained in this study.

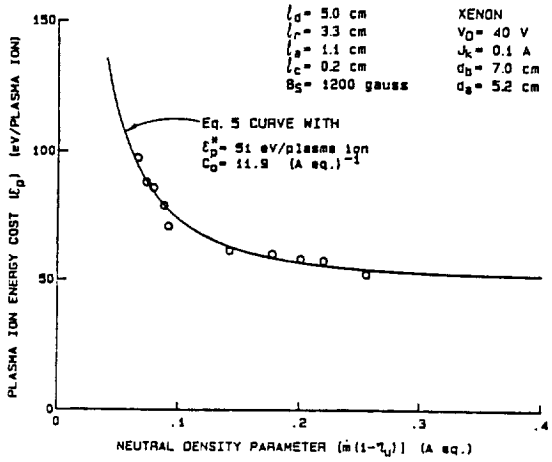

Fig. 5. Typical Discharge Chamber Performance Data

The primary electron utilization factor C_0 like the one computed from the data of Fig. 5 describes the probability that primary electrons coming from the cathode will have inelastic collisions and lose the bulk of their energy before they reach an anode potential surface. The baseline plasma ion energy cost ϵ_p^* is the average energy cost of producing an ion in the discharge chamber when the neutral density is sufficiently high so that all primary electrons have inelastic collisions before they reach the anode. Ideally, the baseline plasma ion energy cost assumes a nominal value determined by the type of propellant, the discharge voltage V_D, and the potential from which electrons are drawn into the chamber V_c (i.e. the electron source potential). However, if all of the ions produced in the chamber are not measured (e.g. some escape to the hollow cathode or to the anode), or if Maxwellian electrons carry substantial amounts of energy to the anode, the baseline plasma ion energy cost ϵ_p^* will increase above its nominal value. The particular discharge chamber used in these tests was designed so ion losses to the hollow cathode and anode could be made small to minimize the effects of these ion losses on ϵ_p^*.

The other parameter needed to describe discharge chamber performance is the extracted ion fraction f_B (i.e. the fraction of the ions produced in the discharge chamber that are extracted into the beam). This parameter is a measure of the effectiveness of the magnetic field in preventing the ions from reaching discharge chamber surfaces and directing them toward the grids.

The advantage of describing discharge chamber performance in terms of the energy cost of a plasma ion (i.e. C_0 and ϵ_p^*) and the extracted ion fraction f_B is that they make it possible to identify the mechanisms responsible for changes in discharge chamber performance. For example one can determine if changing the location of the anode causes a detrimental change in performance and if this change is due to increased losses of primary electrons (a decrease in C_0), increased losses of ions to hollow cathode or anode surfaces or an increase in the average energy of Maxwellian electrons being collected by the anode (an increase in ϵ_p^*) or increased losses of ions to some other discharge chamber surface (a decrease in f_B).

It should be noted that a knowledge of the values of ϵ_p^*, C_0 and f_B is sufficient to enable one to compute the associated beam ion energy costs of a chamber as a function of propellant utilization efficiency.[4]

Effects of Anode Position

The results of the study conducted by Hiatt[1] showed that discharge chamber performance improves when the anode is moved downstream of the axial reference location up to the point where the discharge is on the verge of extinction. It was suggested that the downstream movement of the anode improved performance because it reduced the loss rates of higher energy Maxwellian and primary electrons, to the anode up to the point where the orthogonal line integral of the magnetic field between the virtual cathode and anode surfaces became too great and the discharge would go out. Similar results were also observed in the present study where a hollow cathode was used in place of the filament cathode. However, in the case of the hollow cathode experiments, an actual extinction of the discharge was not observed. Rather the discharge current would decrease until it became too small to produce significant numbers of ions as the anode was moved downstream and the discharge voltage and propellant flowrate were held constant. The higher the discharge voltage and propellant flowrate the further downstream the anode could be moved before this situation developed.

Typical experimental results obtained during a test to investigate the effects of moving the anode on discharge chamber performance are presented in Fig. 6. These results are qualitatively similar to those obtained by Hiatt[1] in a similar discharge chamber equipped with a filament cathode. The data were recorded using a chamber with the dimensions shown in the legend when the magnetic surface flux density B_S was 1200 gauss. The data points shown at ℓ_a = 0.96 cm were recorded with the anode just upstream of the operating point where the maximum discharge current that could be drawn dropped precipitously at nominal discharge voltage and total flow conditions (40 V and 150 mA eq (Xe)). It is noted that low values of ϵ_p^*, and high values of C_0 and f_B are desirable so operation with ℓ_a far downstream (large values of ℓ_a) is preferred.

Because the propellant, discharge voltage and electron source potential (keeper voltage) were constant for these tests it is argued that the decrease in baseline plasma ion energy cost with downstream anode movement is caused by the decrease in the average energy of Maxwellian electrons being collected at the anode that has been observed previously.[1,4] This preferential collection of progressively lower energy electrons as the anode is moved downstream occurs because the momentum transfer collision cross section for electrons with atoms and ions increases as electron energy decreases. Hence as the virtual anode is moved further from the virtual cathode (i.e. the anode is moved downstream) electrons which have the lowest energies (and therefore have many collisions) are most likely to migrate across magnetic field lines and reach the anode. Thus, downstream movement of the anode reduces the average energy of the Maxwellian electrons reaching the anode and this induces the decrease in ϵ_p^* as ℓ_a is increased.

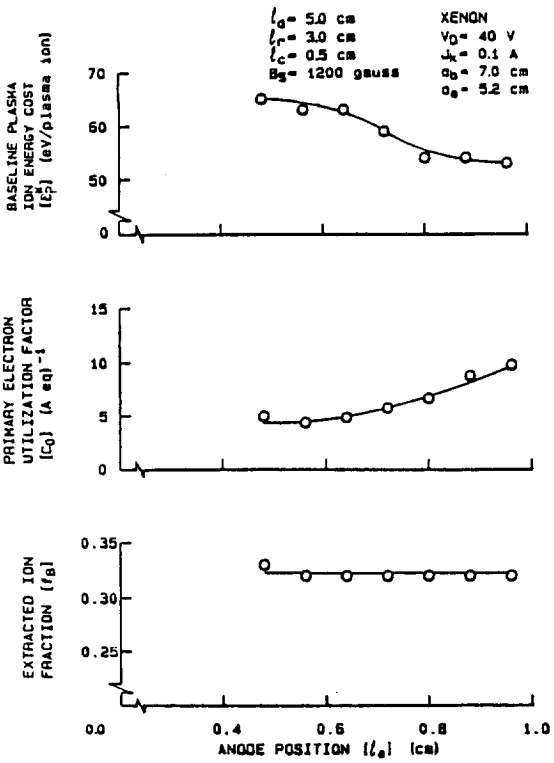

Fig. 6. Effect of Anode Position on Discharge Chamber Performance Parameters

The primary electron utilization factor (C_0) is observed to increase as the anode was moved downstream. Because the primary electrons have an energy that is high compared to that of the Maxwellian electrons, they have low collision probabilities and therefore cannot cross field lines easily. As the anode is positioned further downstream the number of field lines that must be crossed to reach the anode increases, therefore the primary electron loss rate decreases and the primary electron utilization factor increases to reflect this.

Figure 6 shows the extracted ion fraction remains constant as the anode is moved downstream. This indicates that the total ion production rate and the beam current are changing at the same rate. During typical experiments the beam current was observed to increase as the anode was moved downstream and the discharge voltage, current and total flowrate were held constant (accomplished by adjusting the flow distribution). It is obvious from looking at Fig. 6 that this increase in beam current occurred because downstream anode movement induces an increase in C_0, a decrease in ϵ_p^* and no change in f_B. Physically this occurs because the energy in both the primary and Maxwellian electron groups is being better utilized to make ions and the fraction of these ions that escape the discharge chamber into the beam remains constant as the anode is moved downstream.

The Comparative Behavior of Refractory Filament and Hollow Cathodes on Performance

When a filament cathode electron source is used one can control the shape and location of the region from which primary electrons are supplied to the discharge, but with a conventional hollow cathode one is limited to electron emission from a point on the discharge chamber centerline. A question that arises is whether a filament cathode emitting electrons from the same point on a discharge chamber centerline would give the same performance as a hollow cathode. In order to address this question an experiment was conducted in which a discharge chamber was operated using a hollow cathode and then a small diameter (2 mm) coiled filament positioned at the axial location previously occupied by the hollow cathode orifice. The discharge chamber remained unchanged except for the cathode substitution.

Figure 7 shows the comparative plasma ion energy cost vs. neutral density parameter and extracted ion fraction data measured with the cathodes positioned downstream of the cusp at ℓ_c = 0.2 cm and the rest of the discharge chamber parameters as listed in the legend. The data show no difference in either the extracted ion fraction or the primary electron utilization factor, however, the baseline plasma ion energy cost for the hollow cathode is approximately twice that of the filament cathode. These large differences in baseline plasma ion energy cost can be accounted for by recognizing that the primary electrons acquire an energy approximately equal to the difference between the anode and electron source potentials. In the case of the filament cathode this would be the potential difference between the filament surface and the anode (i.e. the discharge voltage). For the hollow cathode, where it might be assumed the electron source potential is about equal to the keeper potential (V_K) the appropriate potential difference would be the difference between the discharge and keeper voltages.[4] In this case the plasma ion energy cost would be given by

$$\epsilon_p = \frac{(V_D - V_K)(J_D - J_P)}{J_P} \quad (6)$$

The difference in plasma ion energy costs given by this equation and by Eq. 2 represents the energy cost per plasma ion being used to operate the hollow cathode.

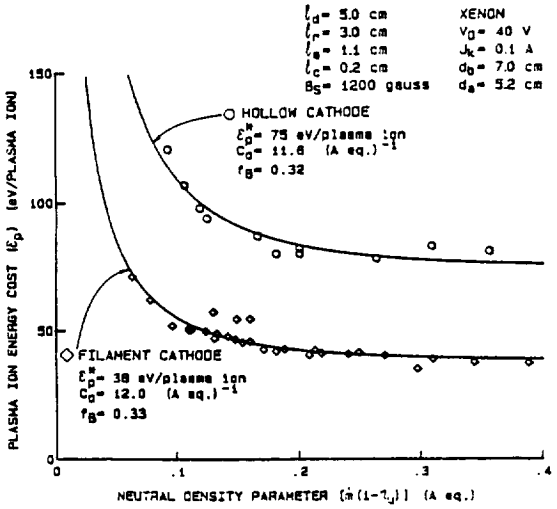

Fig. 7. Hollow Cathode/Filament Cathode Performance Comparison

During the conduct of the test with the hollow cathode, the keeper voltage generally varied from 12 V at low neutral densities (high cathode flows) to 20 V at high neutral densities (low cathode flows). If the electron source potential was assumed to be equal to that of the keeper at high neutral densities (~20 V) and Eq. 6 was used to calculate the plasma ion energy cost, the hollow cathode data (circular symbols) shown in Fig. 8 were computed. These data show good agreement between all parameters (ϵ_p^*, C_0 and f_B) for the filament and hollow cathode cases thereby suggesting the hollow cathode operating power has been properly removed from baseline plasma ion energy cost. This suggests that discharge chamber performance with a hollow cathode and with a filament cathode are comparable if hollow cathode operating power is accounted for properly. It is noted that using the keeper voltages measured at each discharge

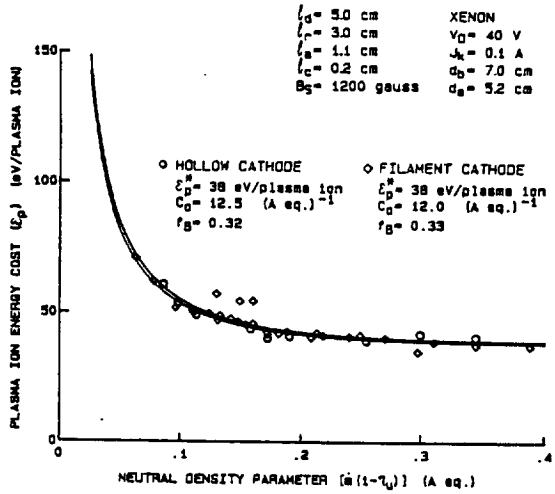

Fig. 8. Hollow Cathode/Filament Cathode Performance Comparison (with Keeper Potential Correction)

current condition rather than the constant (20 V) value did not result in the same degree of agreement as that shown in Fig. 8. When the variable keeper voltage values were used in Eq. 6 the values of both ϵ_p^* and C_0 determined by the least squares fitting of the data for the hollow cathode departed from those for the filament cathode. While it may be that electrons are being supplied from this higher potential as keeper voltage changes, more research into the subject of hollow cathode vs. filament cathode effects on discharge chamber performance to enhance understanding of the phenomena that are occurring is considered desirable.

Effects of Hollow Cathode Axial Position

Tests were conducted in which the anode position and magnetic field configuration were fixed and the effect of hollow cathode movement along the thruster centerline was examined. Discharge chamber performance plots like those in Fig. 5 were generated at each cathode position and discharge chamber performance parameters (ϵ_p^*, C_0 and f_B) were determined from these data using Eqs. 3 and 5. Figure 9 shows the variation in these parameters as a function of hollow cathode position over the range $-0.6 \leq \ell_c \leq 0.5$ cm. These data suggest the primary electron utilization factor is not affected by cathode position but both baseline plasma ion energy cost and extracted ion fraction increase as the cathode is moved upstream of the reference (central ring cusp) location. One of these effects is beneficial (increased extracted ion fraction) and the other is detrimental (increased baseline plasma ion energy cost). The fact that these curves show similar behavior suggests both parameters are being affected by a common phenomenon. The behavior shown in Fig. 9 could be explained qualitatively if upstream movement of the hollow cathode causes a fraction of the ions that were being lost to the chamber walls to be lost to the hollow cathode itself. This effect would cause both parameters to increase with upstream cathode movement because ions lost to the cathode are not measured and this therefore causes a decrease in the measured ion production J_p which appears in the denominator of the expressions from which these parameters (Eqs. 2 and 3) are computed. A development in Appendix A shows in fact that the values of these parameters are related by the equation

$$f_B = \frac{\hat{f}_B}{\hat{\epsilon}_p^*}\,\epsilon_p^* \qquad (7)$$

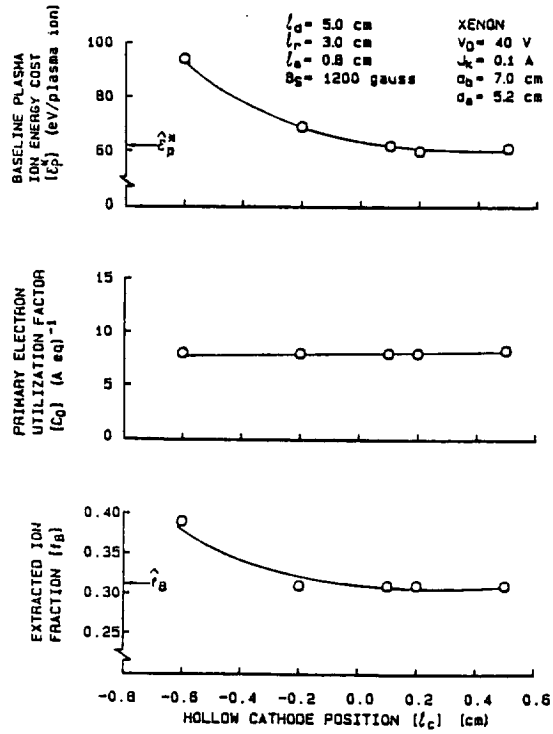

Fig. 9. Effect of Centerline Hollow Cathode Axial Position on Discharge Chamber Performance Parameters

where $\hat{f}_B$ and $\hat{\epsilon}_p^*$ (identified in Fig. 9) are the values of the parameters associated with the cathode positioned in the downstream region where the ions lost to the hollow cathode are low. Finally, it is noted that the use of Eq. 6 rather than Eq. 2 to determine values of ϵ_p^* from which values of ϵ_p^* are computed as a function of cathode position (i.e. to account for losses associated with the electron source potential) causes the data from these tests to fall into even better quantitative agreement with Eq. 7. All of these results taken together suggest that the increase in extracted ion fraction induced by upstream cathode movement is artificial and is compensated by a corresponding increase in baseline plasma ion energy cost to the point where no substantial net effect on beam ion energy cost is realized.

The reason why ion losses to the cathode increase as it is moved upstream can be understood by considering the centerline magnetic flux density profile shown in Fig. 10. These measurements, which

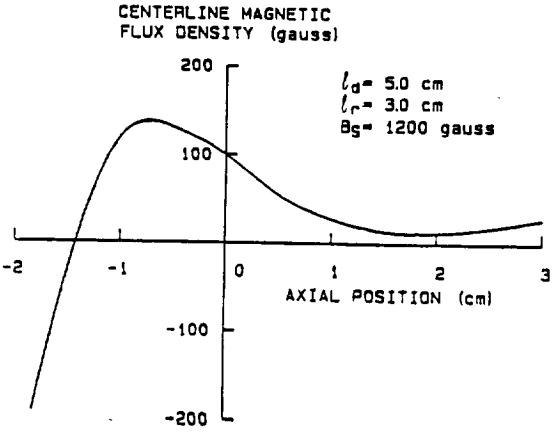

Fig. 10. Centerline Magnetic Flux Density Profile

were made using a gaussmeter, show the cathode is moving into a progressively higher magnetic flux density environment as it is moved upstream. This would be expected to confine electrons (and therefore ions) progressively closer to the cathode and would promote ion losses to cathode surfaces at the expense of ion losses to the chamber walls.

It is noted that the data of Fig. 9 are limited to upstream cathode positions greater than -0.6 cm and Fig. 10 shows this is a region of negative flux density gradient. Movement of the hollow cathode upstream of the point of maximum flux density (~ -0.8 cm), however, caused the performance of the ion source to degrade rapidly because of what appeared to be a dramatic increase in the baseline plasma ion energy cost that overshadowed corresponding modest changes in extracted ion fraction.[2] Thus test results obtained by moving the hollow cathode axially suggest overall discharge chamber performance as reflected in beam ion energy costs, which vary to first order as ϵ_p/f_B, is unaffected by cathode position as long as it is downstream of the extreme, centerline flux density point. As the cathode is moved into regions of higher flux density, however, a greater fraction of the ions produced near the cathode appear to go to the cathode rather than to the chamber walls.

Magnetic Field Effects

The magnetic field configuration in a discharge chamber is important because it must contain the ions away from the chamber walls and near the screen grid where they can be extracted into the beam. Two criteria associated with the magnetic field that should be met for a good design are: 1) a sufficiently high magnetic flux density near the surface of the discharge chamber walls to ensure proper ion containment and 2) proper positioning of the ring magnet so the virtual anode field line will intersect the outer most ring of holes in the screen grid. These criteria were difficult to meet simultaneously with the small diameter discharge chamber used in these tests because fringing fields tended to penetrate deep into the chamber and reduce the low field strength volume in it. However, effects associated with these criteria were investigated by changing the flux density of the magnets and the axial location of the central ring magnet (i.e. varying ℓ_r shown in Fig. 1).

When the magnetic flux density measured at the surface of the steel strips and washer on the magnets (Fig. 1) was varied from 350 gauss to 2700 gauss the discharge chamber performance parameters varied in the manner shown in Fig. 11. These data suggest that increased magnetic flux density induces 1) slightly reduced energy losses through Maxwellian electron losses to the anode (ϵ_p decreases with B_s), 2) improved primary electron containment (C_0 increases with B_s) and 3) improved ion containment (f_B increases with B_s). All of these trends improve performance and they are most significant over the magnetic flux density range from 350 to 1200 gauss. Beyond 1200 gauss the improvements in all of the parameters appear to be small.

Some insight into these trends can be gained by considering a typical pseudo iron filings map (Fig. 3 - the shape of the lines in this figure do not change significantly with flux density) and pertinent magnetic flux density contour maps (Fig. 12) associated with the discharge chamber. In viewing Fig. 3 it should be recognized that ions and electrons can diffuse readily along field lines and with difficulty across them. They can therefore diffuse readily (at the ambipolar diffusion rate) to cusps where electrons will generally be reflected because the pole pieces do not serve as anodes in this thruster and significant numbers of ions will be lost to the ring magnet surface. This ion loss rate is believed to have a relatively weak dependency on magnet strength. Ions and electrons can also be lost by diffusing more slowly (at the Bohm diffusion rate) across field lines; electrons being lost to the anode

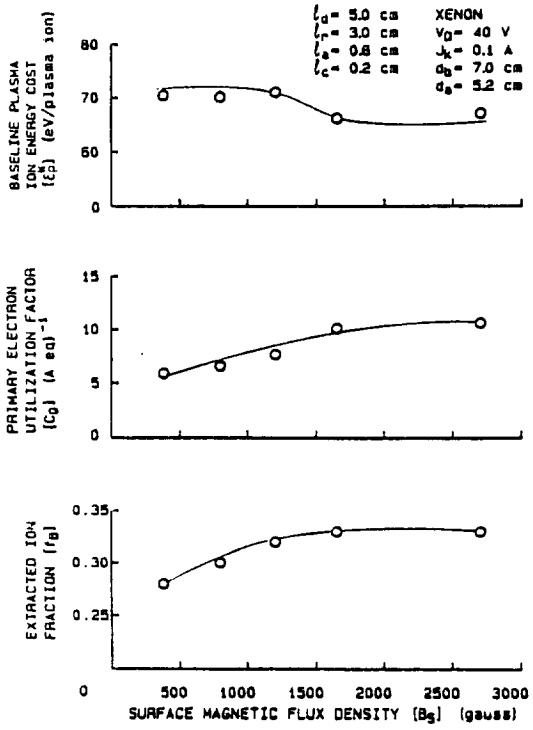

Fig. 11. Effect of Magnet Strength on Discharge Chamber Performance Parameters

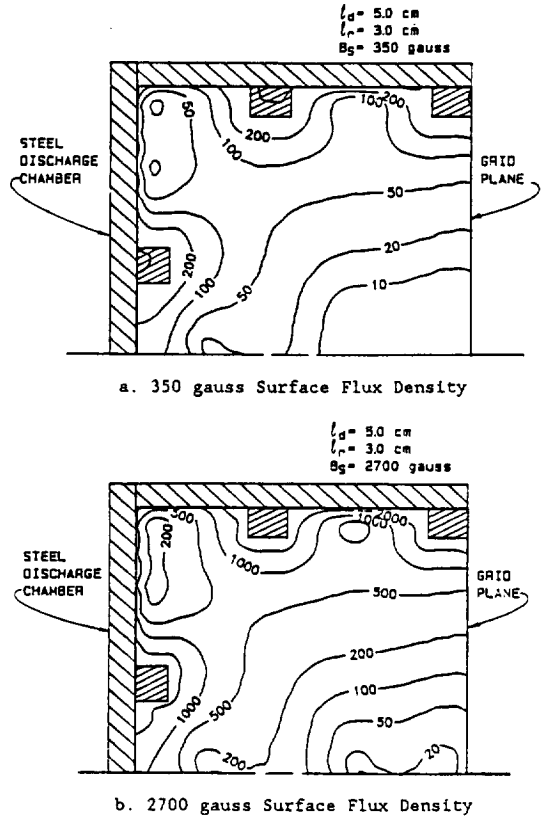

a. 350 gauss Surface Flux Density

b. 2700 gauss Surface Flux Density

Fig. 12. Magnetic Flux Density Contour Maps

once they reach the field line which intersects the anode and ions being lost to the discharge chamber walls. This ion loss mechanism (Bohm diffusion) decreases as the magnetic flux density increases but at some magnetic field strength (presumably near 1200 gauss in the case of the chamber configuration associated with the data of Fig. 11) the ion loss rate to the walls becomes small compared to the ion loss rate through the cusps.

Figure 12 contains magnetic flux density contour maps which show the effects of surface flux density B_S on magnetic flux density in the discharge chamber. Comparison of Figs. 12a and 12b shows considerably higher flux densities develop throughout the chamber when the surface flux density B_S is increased from 350 to 2700 gauss. Because the Bohm diffusion coefficient varies inversely with flux density, electron and ion flow across field lines to the anode and to the chamber wall will be substantially less in the high flux density case.

Positioning of the ring magnet so that the virtual anode field line intersects the outermost ring of holes in the screen grid is also important in determining the overall performance of an ion thruster. When the virtual anode field line intersects these outer holes, a larger fraction of the neutrals are utilized because they cannot escape the chamber without passing through a zone where they can be ionized. Utilization of these additional neutrals increases the beam current which can be extracted from the discharge plasma and increases the uniformity of the beam current density profile. The parameter that describes the uniformity of the beam current density and thereby infers the proximity of the virtual anode field line surface of revolution to the surface of revolution of the field line passing through the outermost ring of holes is the beam flatness parameter (the ratio of average-to-peak beam current density measured near the grids).

In this study the central ring magnet was moved axially (ℓ_r of Fig. 1 was varied) in order to induce some degree of movement in the virtual anode field line and the beam flatness parameter and discharge chamber performance parameters were measured as a function of this movement. The effects of varying ℓ_r from 2.6 to 3.6 cm on beam flatness parameter and the discharge chamber performance parameters ϵ_p^*, C_Q and f_β are shown in Figs. 13 and 14 for the case where the anode and cathode positions (ℓ_a and ℓ_c in Fig. 1) were held constant relative to the ring magnet being moved. The test was conducted in this way because earlier test had suggested that holding ℓ_a and ℓ_c constant should tend to hold baseline plasma ion energy cost ϵ_p^* and primary electron utilization factor C_Q relatively constant. The tests were conducted using a ring magnet surface flux density of 1200 gauss because lesser values yielded poor performance parameters (Fig. 11) and higher values tended to reduce the volume of the low magnetic flux density volume in the chamber (Fig. 12b). The data presented in Fig. 13 show an increase in the flatness parameter as the ring magnet position is moved upstream, presumably because more of the screen grid is exposed to the uniform density discharge chamber plasma. This suggests the optics system is being used more effectively and less unionized propellant is being lost because of a non-uniform ionizing plasma across the grids (a fact that was also confirmed by independent propellant utilization efficiency measurements).

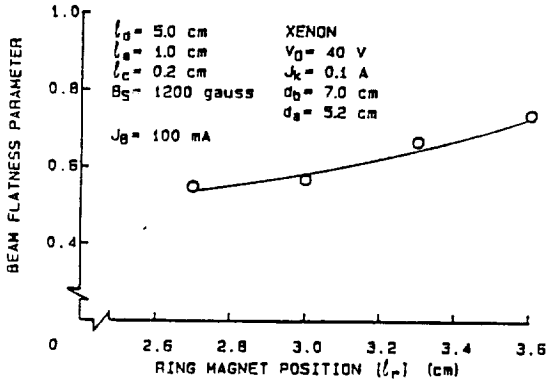

Fig. 13. Effect of Ring Magnet Position on Beam Flatness Parameter

If the rate at which ions are being extracted into the beam increases then one might also assume that a similar increase in the extracted ion fraction should occur. However, the discharge chamber performance data contained in Fig. 14 (bottom plot) show that the opposite has occurred; that the extracted ion fraction decreases as the ring magnet is moved upstream. Examination of the data suggests this occurs because of increased losses to discharge chamber walls. The other performance data in Fig. 14 suggest the baseline plasma ion energy cost goes through a slight minimum and taken together the data suggest there is an optimum ring magnet position near 3.0 cm.

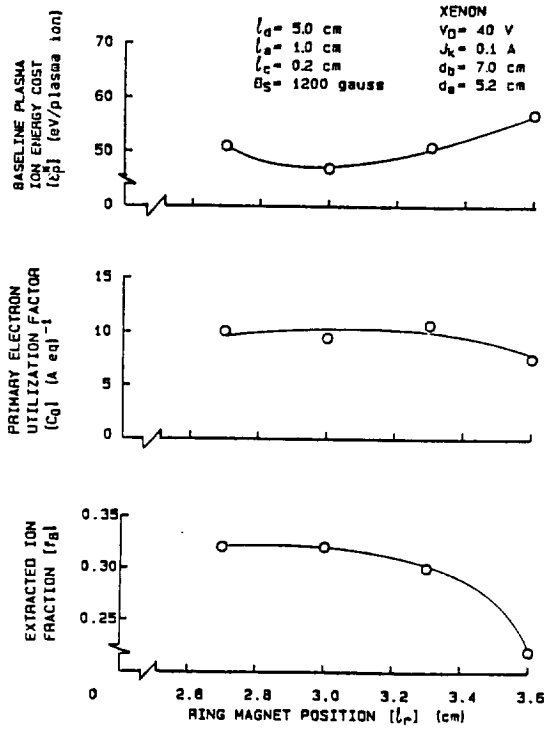

Fig. 14. Effect of Ring Magnet Position on Discharge Chamber Performance Parameters

The reason the extracted ion fraction decreases while the beam flatness parameter increases when the ring cusp is moved upstream to a position 3.6 cm from the grid plane can be seen by comparing the flux density contour map in Fig. 15 with the one in Fig. 4 (which pertains to ℓ_r = 3.0 cm). This comparison shows the magnetic flux density near the discharge chamber wall between the two radially facing ring magnets decreases as the central magnet is moved upstream and this would be expected to facilitate diffusion of ions across field lines to the wall. In fact increasing the value of ℓ_r from 3.0 to 3.6 cm causes the measured ion current going to the discharge chamber wall to increase 30% and this causes the corresponding 30% decrease in the extracted ion fraction shown in Fig. 14. Comparison of Figs. 4 and 15 also indicates the diameter of the lower flux density region near the grids tends to increase as ℓ_r is increased. It is believed that it is this effect that causes the beam flatness parameter to increase with ℓ_r.

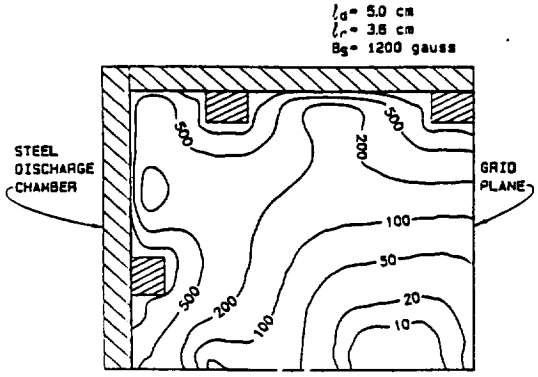

Fig. 15. Magnetic Flux Density Contour Map for ℓ_r = 3.6 cm

In order to produce a magnetic field configuration that would produce good discharge chamber performance and a flat ion beam, the magnetic flux density near the wall should be large enough to prevent ion losses through Bohm diffusion, yet allow the primary electron plasma to occupy a large fraction of the discharge chamber volume adjacent to the grids. In tests conducted with a filament cathode, small diameter ion source, this condition was approached by using a high flux density ring magnet and setting the diameter of the annular zone of electron emission from the cathode to a substantial fraction of the source diameter. This made it possible to achieve relatively high primary electron (and therefore plasma) densities over a rather large volume in the discharge chamber and still limit ion diffusion to the chamber walls. For the present study where a hollow cathode was being used, on the other hand, the point of electron injection remained on the chamber centerline and altering the magnetic field so the volume occupied by the high density plasma could expand also enhanced the rate of ion diffusion to the chamber walls. It is argued therefore, that the simultaneous requirements for low ion diffusion losses and substantial plasma densities near the outermost grid holes tend to be mutually exclusive in small diameter, hollow cathode discharge chambers of the type investigated in this study.

CONCLUSIONS

By examining the effects of changes in hollow cathode discharge chamber performance parameters induced by changes in discharge chamber dimensions and magnetic field strengths it is possible to examine specific physical phenomena that induce changes in discharge chamber performance. This technique has been used to identify the effects induced by changes in anode and hollow cathode position and magnetic field strength and geometry on the performance of a ring cusp discharge chamber with a hollow cathode electron source, three magnet rings, and a 7 cm dia beam.

Results obtained with the anode positioned downstream of a ring cusp in a hollow cathode equipped discharge chamber are qualitatively similar to those obtained by Hiatt[1] using a discharge chamber with a similar beam diameter and a refractory filament cathode. Movement of the anode downstream of the ring cusp toward the grids reduces the primary electron losses to the anode and causes the primary electron utilization factor C_0 to increase continuously up to the point where the discharge impedance becomes so great that significant discharge currents can no longer be drawn without increasing the discharge voltage. When the hollow cathode is moved along the chamber centerline the extracted ion fraction and baseline plasma ion energy cost change in such a way that their combined effect on performance is almost nil provided the cathode is not moved upstream of the peak centerline magnetic flux density. Movement upstream of this peak causes a rapid degradation in performance as a result of ion recombination on hollow cathode surfaces.

An increase in the surface flux density of the ring magnets improves the confinement of both primary electrons and ions up to a surface flux density of ~ 1200 gauss. Increases in surface flux density beyond this value induce negligible additional improvement in the confinement of each species. Upstream movement of the central ring magnet in the discharge chamber introduces competing performance effects. It causes the volume of the ionizing plasma adjacent to the grids to increase while at the same time allowing increased ion losses to the discharge chamber walls in the region between the downstream and central magnet rings.

When a small diameter filament electron source is substituted for a hollow cathode the primary electron confinement and the extracted ion fraction characteristics of the ion source are unaffected but the baseline energy cost of producing plasma ions decreases by an amount equal approximately to the keeper voltage.

REFERENCES

1. Hiatt, J. M. and Wilbur, P. J., "Ring Cusp Discharge Chamber Performance Optimization," Journal of Propulsion and Power, Vol. 2, No. 5, Sept.-Oct. 1986, pp. 390-397.

2. Vaughn, J. A., "8 cm Dia. Ring Cusp Discharge Chamber Research," appears in "Advanced Electric Propulsion Research," NASA CR-182130, P. J. Wilbur, ed., pp. 1-52, Jan. 1988.

3. Arakawa, Y. and Wilbur, P. J., "Discharge Plasma Calculations in Cusped Ion Thrusters Using the Finite Element Method," Paper 88-079, 20th International Electric Propulsion Conference, Garmisch-Partenkirchen, West Germany, Oct. 3-6, 1988.

4. Brophy, J. R., "Ion Thruster Perfqrmance Model," NASA CR-174810, December, 1984.

APPENDIX A

The Effects of Ion Losses to Cathode or Anode Surfaces on Discharge Chamber Performance Parameters

When ions produced in a discharge chamber are lost to an anode or cathode surface, they cannot be measured because they cannot be distinguished from electrons that must flow to and from these surfaces to sustain the plasma discharge. Because of this a discharge chamber alteration that causes ions, which had been going to a chamber wall where they could be measured, to go instead to a cathode or anode surface would cause an apparent increase in both the extracted ion fraction f_B and the baseline plasma ion energy cost ϵ_p. In order to establish a relationship between the apparent and true values of these parameters the following definitions are offered:

- $\hat{\epsilon}_P$ • The true plasma ion energy cost (based on all ions produced whether they can be measured or not),
- ϵ_P • The apparent or measured plasma ion energy cost (based only on the ion currents going to surfaces where measurements can be made),
- J_B, J_W, J_S • Measured beam current, wall current, and screen current, respectively,
- J_L • Ion loss current that cannot be measured (i.e. going to a cathode or anode surface),
- $\hat{f}_B$ • The true extracted ion fraction (based on all ions produced),

f_B = The apparent or measured extracted ion fraction (based only on the ion current that can be measured).

Since the power being used to create the plasma ions is the same regardless of the accounting scheme used one can write

$$P = (J_B + J_S + J_W)\ \epsilon_P = (J_B + J_S + J_W + J_L)\ \hat{\epsilon}_P. \quad (A1)$$

Further, the true and apparent extracted ion fractions are given by:

$$\hat{f}_B = \frac{J_B}{(J_B + J_S + J_W + J_L)} \quad (A2)$$

and

$$f_B = \frac{J_B}{(J_B + J_S + J_W)}. \quad (A3)$$

Combining Eqs. A1, A2 and A3 to eliminate the currents one obtains

$$\frac{\hat{\epsilon}_P}{\epsilon_P} = \frac{\hat{f}_B}{f_B} \quad (A4)$$

This equation can be written in terms of the baseline plasma ion energy cost (ϵ_P^*) using Eq. 5 and since the primary electron utilization factor C_Q is not affected by ion losses to the anode or cathode (see Fig. 9), the resulting equation can be simplified further to obtain

$$f_B = \frac{\hat{f}_B}{\hat{\epsilon}_P^*}\ \epsilon_P^*. \quad (A5)$$

Hence plasma ion losses to anode or cathode surfaces will induce increases in apparent extracted ion fraction and apparent baseline plasma ion energy cost that are proportional to each other.